

## Accepted Manuscript

Contact stresses in adhesive joints due to differential thermal expansion with the adherends

Annalisa Franco, Gianni Royer-Carfagni

PII: S0020-7683(16)00104-9  
DOI: [10.1016/j.ijsolstr.2016.02.036](https://doi.org/10.1016/j.ijsolstr.2016.02.036)  
Reference: SAS 9081



To appear in: *International Journal of Solids and Structures*

Received date: 12 June 2015  
Revised date: 22 January 2016  
Accepted date: 25 February 2016

Please cite this article as: Annalisa Franco, Gianni Royer-Carfagni, Contact stresses in adhesive joints due to differential thermal expansion with the adherends, *International Journal of Solids and Structures* (2016), doi: [10.1016/j.ijsolstr.2016.02.036](https://doi.org/10.1016/j.ijsolstr.2016.02.036)

This is a PDF file of an unedited manuscript that has been accepted for publication. As a service to our customers we are providing this early version of the manuscript. The manuscript will undergo copyediting, typesetting, and review of the resulting proof before it is published in its final form. Please note that during the production process errors may be discovered which could affect the content, and all legal disclaimers that apply to the journal pertain.

# Contact stresses in adhesive joints due to differential thermal expansion with the adherends

Annalisa Franco<sup>a</sup>, Gianni Royer-Carfagni<sup>b,\*</sup>

<sup>a</sup>*Department of Industrial Engineering, University of Parma, Parco Area delle Scienze 181/A, I 43100 Parma, Italy*

<sup>b</sup>*Department of Industrial Engineering, University of Parma, Parco Area delle Scienze 181/A, I 43100 Parma, Italy*

---

## Abstract

The contact stresses in a bonded joint due to differential thermal expansions are calculated by considering the adhesive as an elastic rectangle confined by plates representing the adherends. The interface is cohesive in type, so that the contact area is a perfectly adherent region surrounded by cohesive areas where slip occurs at constant shear-stress. The problem is formulated in terms of Papkovitch-Fadle eigenfunctions, which satisfy the boundary conditions on the stress free edges. The resulting integral equations are solved with the Jacobi integration formula. The size of the cohesive zone, which is determined by imposing the finiteness of the contact stresses at the frontier with the bonded region, depends upon the length and height of the joint. In very long joints the result tends to the technical rule of thumb traditionally employed to design such joints, but for intermediate lengths the elastic solution is quite different.

*Keywords:* Adhesive joint, differential thermal expansion, cohesive zone, contact stresses, Papkovitch-Fadle eigenfunctions.

---



---

\*Corresponding Author. Tel.: +39 0521 906066; fax: +39 0521 905705

*Email addresses:* [annalisa.franco@unipr.it](mailto:annalisa.franco@unipr.it) (Annalisa Franco), [gianni.royer@unipr.it](mailto:gianni.royer@unipr.it) (Gianni Royer-Carfagni)

Notation			
$\alpha_p, \alpha_r$	Coefficient of thermal expansion of plates and rectangle.	$p_T$	the integral equation
$\alpha_{st}, \alpha_{gl}, \alpha_{al}, \alpha_{si}$	Coefficient of thermal expansion of steel, glass, aluminum and silicone.	$q$	Uniform pressure
$\delta$	Cohesive length in the simple model	$u_x, u_y$	Constant shear stress
$\lambda_n$	Non zero complex roots of the equation $\sin 2\lambda_n + 2\lambda_n = 0$	$w_i^{\alpha, \beta}$	Displacements
$\nu$	Poisson's ratio	$A_n$	Weights of the Jacobi integration formula ( $i = 1, \dots, n_1$ )
$\sigma_{xx}, \sigma_{xz}, \sigma_{zz}$	Stresses	$D$	Unknown complex constants ( $n = -\infty, \dots, -1, 1, \dots, \infty$ )
$\theta$	Shear function	$E$	Real constant
$\varepsilon_p$	Thermal deformation in the plate	$F$	Young's Modulus of the rectangle
$\varepsilon_r$	Thermal deformation in the rectangular domain	$G$	Kernel
$\varepsilon_T$	Thermal deformation	$H$	Shear modulus
$\Delta$	Uniform displacement	$H(y, z)$	Height of the elastic rectangle
$\Omega, \Psi$	Stress functions	$I_0, I_1$	Kernel
$a$	Aspect ratio	$J_0$	Modified Bessel functions
$b$	Width of the elastic rectangle	$K$	Bessel functions
$c$	Half length of the adhesive portion	$K_{II}$	Kernel
$f_{1n}, f_{2n}$	Papkovich-Fadle eigenfunctions	$L^0, L^1, L^2$	Mode II stress intensity factor
$h$	Half width of the elastic rectangle	$M^0$	Kernels
$n_1$	Number of equations approximating	$N$	Kernel
		$P_n^{\alpha, \beta}$	Jacobi polynomial of the first kind
		$Q_1, Q_2$	Shear functions

## 1. Introduction

Adhesive bonded joints play a significant role in the development and production of different-in-type structures, in the aerospace and automotive industries as well as in the electronic technology. In the building industry, structural façades make use of high performance adhesives to fix glass, or other materials, to a rear frame *in lieu* of gaskets or other mechanical attachments. Indeed, metal and glass are frequently glued together in order to avoid the high stress concentrations associated with bolt holes. Apart from the effects of the dead and service loads, the state of stress in the adhesive joints may become critical because of the differential thermal expansion of the adherends and of the adhesive itself.

Since the adherends may present different coefficients of thermal expansion, in the design phase a great attention is paid to their repeated expansions and contractions due to cyclic

temperature variations. Consequently, the adhesive thickness is sized to accommodate these movements, as well as to compensate for flatness tolerances between the adherends. However, quite surprisingly, the thermal straining of the adhesive layer itself is most of the time neglected, although its coefficient of thermal expansion can be orders of magnitude greater than that of the adherends. Just to illustrate, reference can be made to the case of united cells for structural glazing, obtained by bonding glass panels to a metallic frame with structural silicone. Technical guidelines and datasheets for adhesives (3M, 2015; DowCorning®, 2015; ASTM C1401-14, 2014; ETAG 002, 2012) prescribe for the adhesive joint a minimum thickness (in general 6 mm), or a maximum strain of 10 – 15%. Such a limit has to comply with the relative movement of the metallic frame (typically made of steel or aluminum) with respect to the glass panel, due to their different thermal expansion<sup>1</sup>. However, the aforementioned guidelines never mention the thermal dilatation of the structural silicone, although its coefficient of thermal expansion is much greater than that of the adherends<sup>2</sup>.

The aim of this article is to accurately characterize the role of the adhesive when the joint undergoes a temperature variation. The model problem is that of an elastic rectangle (the adhesive) in plain strain, confined by two plates (the adherends), under a uniform thermal variation  $\Delta T$ . If one refers to a typical situation, the confining layers are made of, say, steel and glass, whereas the elastic rectangle represents the structural silicone. Since the adherends have quite similar coefficients of thermal expansion, one can neglect their difference with respect to the much higher thermal deformation of the adhesive, and assume the same thermal strain  $\epsilon_p = \alpha_p \Delta T$  in the confining plates for any temperature variation. On the other hand, the thermal strain  $\epsilon_r = \alpha_r \Delta T$  in the adhesive is much higher. With an elementary argument based upon superposition of effects, schematically illustrated in Figure 1, one can consider the case of an elastic rectangle in contact with two layers undergoing the same

---

<sup>1</sup>Typical coefficients of thermal expansion are  $\alpha_{st} = 10.5 \cdot 10^{-6} \text{ }^\circ\text{C}^{-1}$  (ferritic stainless steel),  $\alpha_{al} = 23.2 \cdot 10^{-6} \text{ }^\circ\text{C}^{-1}$  (aluminum),  $\alpha_{gl} = 9 \cdot 10^{-6} \text{ }^\circ\text{C}^{-1}$  (glass).

<sup>2</sup>A typical coefficient of thermal expansion for a commercial type of structural silicone is  $\alpha_{si} \simeq 290 \cdot 10^{-6} \text{ }^\circ\text{C}^{-1}$ .

thermal strain  $\varepsilon_T = \varepsilon_p - \varepsilon_r = (\alpha_p - \alpha_r)\Delta T$ , in addition to the case in which all the constituents undergo the same thermal deformation  $\varepsilon_r$ . Clearly, only the first case is of importance, because the second condition is stress-free.

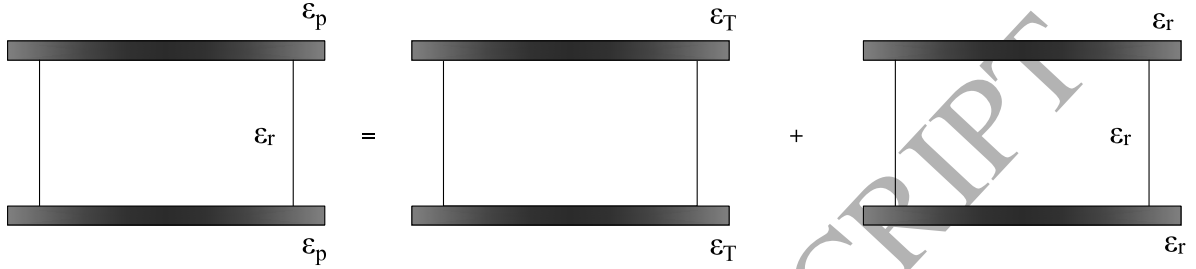


Figure 1: A bonded joint subject to a thermal mismatch. Superposition of the effects of an elastic rectangle confined by two deforming layers, and of the condition in which all the constituents undergo the same thermal deformation.

An expansion (or contraction) of the external layers causes the adhesive interlayer to undergo a state of stress at the interface that can produce partial debonding. Such process is governed by the interfacial bond strength, which is in general correlated with the relative displacement between the adhesive and the adherend.

While investigating the adhesion properties between glass and polymers through TCT (Through-Cracked-Tensile) tests, Ferretti et al. (2012) observed that the force-displacement diagram showed a peak followed by a horizontal *plateau* associated to progressive delamination. Analysis of these tests has shown that during the delamination process, the glass-polymer relative displacement increases while the corresponding shear stress remains almost constant. This steady state regime has also been observed by other authors, for other types of polymeric interlayer (Delincé et al., 2008; Muralidhar et al., 2000). There is a general agreement that the strength of an adhesive joint can be characterized through a bond-stress vs. relative-displacement constitutive law. Many models for adhesive interfaces have been developed since the 1960s and a list of relevant references can be found in Raous (2011). Most of them have focused on the cohesive zone models in the context of fracture mechanics, following the seminal works by Dugdale (1960), Barenblatt (1962), Needleman (Needleman, 1987,

1990, 1992), for normal-loading conditions, and Tvergaard & Hutchinson (Tvergaard and Hutchinson, 1993, 1994), Xu and Needleman (1994), for mixed-mode loading.

One of the most used model is that by Tvergaard and Hutchinson (1993), who assumed a trapezoidal shear-stress vs. relative-slip constitutive law at the interface, articulated in three phases: a linear ascending branch up to the peak stress, a *plateau* where displacement increases at constant stress and, finally, a linear strain-softening phase approaching the fracture displacement where the stress is null. In certain cases, since the ascending and descending branches can be considered negligible if compared with the width of the intermediate *plateau*, it is reputed to be sufficient to consider the simplest step-wise law to interpret the gradual debonding process (Franco and Royer-Carfagni, 2014a,b).

Other authors have considered the imperfect bonding of two elastic solids through a thin elastic layer, to rigorously derive interface conditions by letting the thickness of the interlayer go to zero. In general, one obtains constitutive relations more complex than the classical ones, in which the local stress is supposed to be a linear function of the relative displacement between the adherends. These methods rely in general on asymptotic expansions, under some basic assumptions about the rescaling of the elastic moduli and the type of strain inside the interlayer. For example, Klarbring (1991) made the hypothesis that the displacement varies linearly and the stress is constant through the interface. The solution was shown to be unique also in the limit of vanishing thickness, resulting in the formation of a boundary layer. An accurate classification was obtained in Benveniste and Miloh (2001), where the authors recognized seven different regimes of interface conditions. In particular, four cases are distinguished for stiff interfaces, which remarkably have a close remembrance with membrane and classical shell theory. This means that the curvature of the interface plays a dominant role in equilibrating the applied loads. The problem was successively investigated by Hashin (2002). In general, for very compliant interphases there are significant displacement jumps and negligible traction jumps, while for very stiff interphases the situation is reversed, i.e., the displacement jumps are insignificant and the traction jumps may be considerable. For the in-between case, when the interphase and adjacent phase properties are not extremely

different, the usual perfect interface conditions apply in a practical sense. The effects of elastic anisotropy was further studied by Lebon and Rizzoni (2011), by using arguments of asymptotic expansions and energy minimization.

The interface model used here is very simple in type and can be considered, for plane problems, the equivalent of a rigid-plastic interlayer. On the one hand, this type of interface can be considered a first order approximation of the shear vs. slip constitutive equations that are commonly recorded in the technical literature for imperfect interfaces, in particular for problems of FRP reinforcement (Franco and Royer-Carfagni, 2014b). On the other hand, while attempting to solve an elastic problem like the one considered here, using classical methods of linear elasticity theory, some simplifications need to be made to avoid insurmountable analytic complications.

By insight, one should derive the horizontal *plateau* in the assumed stress vs. slip constitutive equation for the interface from the asymptotic expansion of a very thin non-linear elastic interlayer, as its thickness tends to zero. However, the interposed material should be governed by a non-convex type of elastic energy, like the one considered in the seminal work by Ericksen (1975) for the one-dimensional case. More in general, one could represent the interlayer with a non-linear elastic material, which is obviously governed by a non convex potential. In fact as discussed, e.g., in Buonsanti and Royer-Carfagni (2003), by letting some geometric parameters go to zero, one can derive one-dimensional models *à la* Ericksen with non-convex strain energy starting from “genuine” three-dimensional, nonlinear, compressible, elasticity theory. Although such derivation is beyond the scope of this paper, it intuitively suggests new possible approaches and comparisons with the model presented here.

Therefore, the simple step-wise shear-stress vs. relative-slip constitutive law will be assumed in the following for the adhesive/adherend interface. Moreover, since the Young’s modulus of the adherends is several orders of magnitude higher than that of the adhesive, we will neglect the elastic deformation of the confining layers. Such hypotheses are common in the practical design, according to which an estimate of the state of stress in the adhesive can be obtained according to the elementary model schematically represented in Figure 2. Here, it

is assumed that the stress in the adhesive is constant in its height, but it is variable along its width. Denote with  $H$  and  $E$  the height and the Young's modulus of the elastic rectangle, with  $\Delta T$  the temperature variation, with  $\varepsilon_T = (\alpha_p - \alpha_r)\Delta T$  the thermal dilatation of the confining plates (Figure 1), and with  $q$  the “yielding” shear stress at the interface. Therefore, the length  $\delta$  of the cohesive zone where slip occurs to balance the thermal strain  $\varepsilon_T$  can be estimated by

$$\varepsilon_T \frac{E}{1 - \nu^2} = \frac{2q\delta}{H} \Rightarrow \delta = \frac{H}{2} \varepsilon_T \frac{E}{(1 - \nu^2)q}. \quad (1.1)$$

This trivial calculation represents, most of the times, the only technical solution to this problem.

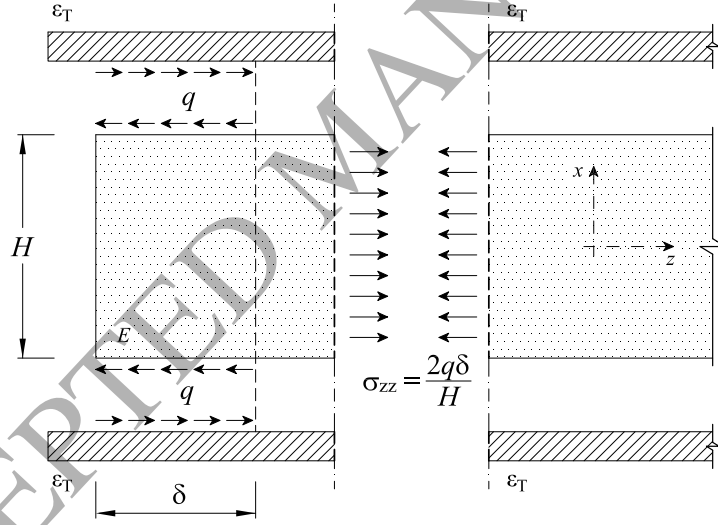


Figure 2: Elementary scheme for the technical calculation of the cohesive (yielded) zone.

To provide a more accurate estimate, we study here the complete elastic problem of a rectangle confined between two expanding elastically-rigid plates. Boundary value problems for elastic rectangular domains have been studied by several authors (Prasad and Dasgupta, 1975; Prasad and Chatterjee, 1973; Chiu et al., 1976; Chatterjee and Prasad, 1973). In particular, Prasad and Dasgupta (1975) studied the boundary value problem in a rectangular



domain compressed by two rigid, rough planes with finite coefficient of friction, where the other set of parallel edges was free from tractions. The study of Prasad and Chatterjee (1973) regarded the problem of the rectangle with different mixed boundary conditions on two parallel edges arising from the compression exerted by two smooth rigid planes, or some periodic arrangement of cracks. Chiu et al. (1976) considered the indentation of an elastic rectangle by rough punches with finite coefficient of friction. In all of these studies, in order to handle the presence of stress free edges, suitable eigenfunctions had to be used (Papkovitch, 1940; Fadle, 1940; Chatterjee and Prasad, 1973).

Following the same rationale, here the contact area is divided into a central perfectly-bonded zone, surrounded by outer regions where slip occurs under constant shear stress. The problem is formulated in terms of Papkovitch-Fadle eigenfunctions (Chatterjee and Prasad, 1973), which satisfy the boundary conditions on the stress free edges. The contact is determined by an integral equation that involves the presence of an unknown constant, whose value determines the size of the cohesive, yielded zone. The extent of such a zone can be determined by imposing the annihilation of the stress intensity factor at the point that separates the bonded from the cohesive zone.

Solutions of the integral equation have been obtained by employing the Jacobi integration formula and exploiting the properties of Jacobi polynomials. A one-factor-at-a-time analysis was then performed to analyze the influence of different geometrical, mechanical, and thermal parameters on the cohesive zone length. The results are in general very different from the elementary deduction of (1.1), but this is found to be the asymptotic limit of the solution of the elastic problem as the width of the rectangle tends to infinity or, equivalently, when its height tends to zero.

## 2. The model problem

The rectangular domain of width  $b = 2h$  and height  $H = 2ah$ , being  $a$  the aspect ratio, represents the undistorted reference configuration of an elastic body in plane strain, with

Young's modulus  $E$  and Poisson's ratio  $\nu$ . As shown in Figure 3, the domain is referred to the Cartesian system of axes  $hx$  and  $hz$  and is confined by two rigid plates at  $z = \pm a$ .

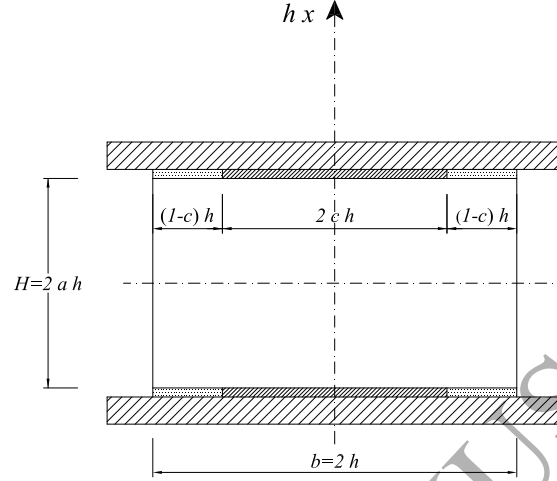


Figure 3: Rectangular reference domain for the elastic body confined by two rigid plates, with indication of the adhesive and cohesive contact zones.

Following the scheme of Figure 1 suppose that, as a consequence of the differential thermal expansion, the strain in the confining plates becomes  $\varepsilon_T$ . The boundary surfaces  $z = \pm 1$  are stress-free, while at  $x = \pm a$  the contact region is composed of an inner adhesive zone  $|z| \leq c$ , where the bonding is perfect, surrounded by cohesive areas,  $c \leq |z| < 1$ , where slip can occur under a constant shear stress  $q$ .

To solve this problem, it is convenient to regard this configuration as the superposition of two states, schematically represented in Figure 4. First, the elastic rectangle is uniformly compressed by the axial stress  $p_T = E\varepsilon_T/[\nu(1 + \nu)]$ , so that its lateral expansion precisely matches with the strain  $\varepsilon_T$ . Because of this the interfacial shear stress is null. In the second step, the compressive stress is removed by an equal but opposite action, represented by the force per unit-thickness  $2hp_T$ , being  $2h$  the rectangle width. The original contact problem can therefore be recovered by the superposition of two subproblems: *i*) an elastic rectangle under the uniform compression  $p_T = E\varepsilon_T/[\nu(1 + \nu)]$ ; *ii*) an elastic rectangle confined by two rigid plates and subject to the traction  $2hp_T$ .

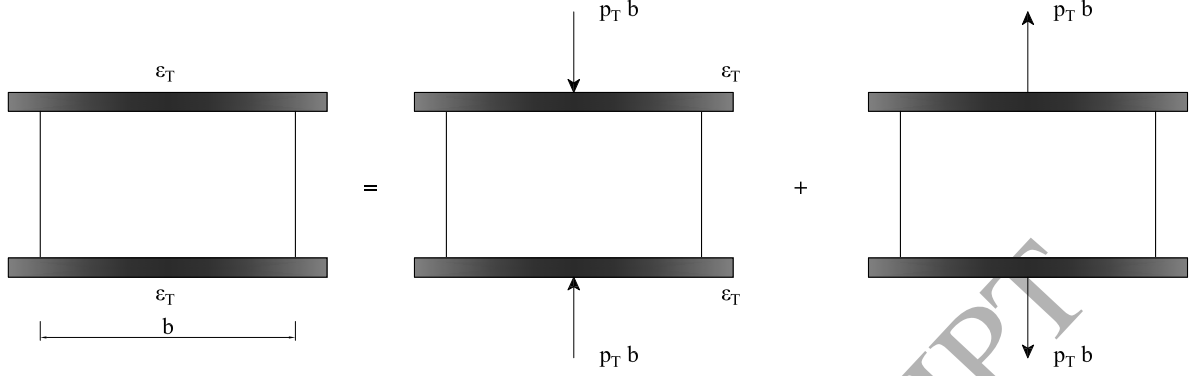


Figure 4: An elastic rectangle confined by two rigid plates undergoing a thermal expansion  $\varepsilon_T$ . Superposition of the effects of a uniformly-compressed rectangle and a confined rectangle under traction.

### 2.1. Subproblem I: elastic rectangle under compression and thermal strain

Since the lateral expansion due to the compressive stress

$$p_T = E \frac{\varepsilon_T}{\nu(1 + \nu)}, \quad (2.2)$$

exactly matches the dilatation of the plate  $\varepsilon_T$ , the state of stress at the interfaces is of the form

$$\sigma_{xx}^I(\pm a, z) = -p_T, \quad (2.3)$$

$$\sigma_{xz}^I(\pm a, z) = 0, \quad (2.4)$$

where the superscript  $I$  evidences the reference to the first subproblem.

### 2.2. Subproblem II: elastic rectangle under traction

When the confining plates are pulled by the force per-unit-thickness  $2h p_T$  (Figure 4), the interface  $z = \pm a$  is formed by the adhesive and cohesive regions indicated in Figure 3, represented by the conditions (superscript  $II$  indicates reference to the second subproblem)

$$u_x^{II}(\pm a, z) = \pm(1 - \nu)\Delta, \quad \text{for } -1 \leq z \leq 1, \quad (2.5)$$

$$u_z^{II}(\pm a, z) = 0, \quad \text{for } 0 \leq |z| \leq c < 1, \quad (2.6)$$

$$\sigma_{xz}^{II}(\pm a, z) = \pm(1 - \nu)q, \quad \text{for } c \leq |z| < 1, \quad (2.7)$$

where  $\Delta$  is a constant to be determined, representing the displacement associated with the tractions  $2h p_T$ , while here  $q$  is representative of the (constant) shear stress in the cohesive zones. For convenience, all quantities have been made dimensionless, so that the units of lengths and stresses are respectively  $h$  and  $2G$ .

The aforementioned boundary conditions allow to write the governing integral equation in terms of the shear stresses in the adhesive and in the cohesive zones. The integral equation involves the parameter  $c$ , which determines the extent of the cohesive zone or, equivalently, the size of the adhesive zone, whose value can be determined by imposing the finiteness of the contact stresses at the frontier between the inner adhesive region and the outer cohesive zones.

It is convenient to expand the solution of Navier's equations for plane strain in the form<sup>3</sup>

$$u_x(x, z) = (1 - \nu)Dx - \sum_n A_n \lambda_n \sinh(\lambda_n x) f_{1n}, \quad (2.8a)$$

$$u_z(x, z) = -\nu Dz - \sum_n A_n \cosh(\lambda_n x) \left[ f'_{1n}(z) + 2(1 - \nu) f'_{2n}(z) \right], \quad (2.8b)$$

where  $D$  is an unknown real constant that represents a uniform traction,  $A_n$  ( $n = -\infty, \dots, -1, 1, \dots, \infty$ ) are unknown complex constants and  $f_{1n}$  and  $f_{2n}$  constitute a set of complex valued Papkovitch-Fadle eigenfunctions, whose expression is given by (A.6) in Appendix A. In equation (2.8b), prime indicates derivative with respect to  $z$ . This set of eigenfunctions satisfies the traction-free conditions on the boundary  $z = \pm 1$ , i.e.,

---

<sup>3</sup>see Appendix A.

$$\sigma_{xz}(x, \pm 1) = \sigma_{zz}(x, \pm 1) = 0, \quad (2.9)$$

provided that  $\sin 2\lambda_n + 2\lambda_n = 0$ . For a discussion of the properties of the eigenfunctions and their adjoints, reference is made to Chatterjee and Prasad (1973) and a (non-exhaustive) summary is reported in Appendix A.

The stresses  $\sigma_{xx}$ ,  $\sigma_{zz}$  and  $\sigma_{xz}$  can be found from (A.10) and are given by

$$\sigma_{xx}(x, z) = D - \sum_n A_n \cosh(\lambda_n x) \lambda_n^2 [f_{1n}(z) - \nu f_{2n}(z)], \quad (2.10a)$$

$$\sigma_{xz}(x, z) = - \sum_n A_n \sinh(\lambda_n x) \lambda_n [f'_{1n}(z) + (1 - \nu) f'_{2n}(z)], \quad (2.10b)$$

$$\sigma_{zz}(x, z) = \sum_n A_n \cosh(\lambda_n x) \lambda_n^2 [f_{1n}(z) + (1 - \nu) f_{2n}(z)], \quad (2.10c)$$

where we recall that the unit of stresses has been chosen to be  $2G$ . In order to satisfy the boundary condition (2.6), two suitable functions, representative of the shear stress, are introduced such that

$$\sigma_{xz}(\pm a, z) = (1 - \nu) \begin{cases} Q_1(z), & 0 \leq z \leq c, \\ Q_2(z), & c \leq z \leq 1. \end{cases} \quad (2.11)$$

By using expression (2.8a) for the displacement, the boundary condition (2.5) leads to the relation

$$\sum_n A_n \lambda_n \sinh(\lambda_n a) f_{1n}(z) = (1 - \nu) [Da - \Delta]. \quad (2.12)$$

Integrating (2.10b) from  $z$  to 1 at  $x = a$  and using (2.11), (2.12) and the relation (A.9), it is possible to obtain the constant  $D$  as

$$Da = \Delta + \nu \int_0^c t Q_1(t) dt + \nu \int_c^1 t Q_2(t) dt. \quad (2.13)$$

The orthonormality conditions (A.8) for the eigenfunctions are used together with (2.11) and (2.12), in order to evaluate the constants  $A_n$ . One eventually obtains

$$A_n \lambda_n \sinh(\lambda_n a) = \frac{1}{2 \cos^2 \lambda_n} \left[ \int_0^c Q_1(t) P(\lambda_n, t) dt + \int_c^1 Q_2(t) P(\lambda_n, t) dt \right], \quad (2.14)$$

where

$$P(\lambda_n, t) = -t \cos(\lambda_n t) + \sin(\lambda_n t) \cot \lambda_n + 2(1-\nu) \frac{\sin(\lambda_n t)}{\lambda_n}. \quad (2.15)$$

Equation (2.14) can then be substituted in the expression (2.8b) for the displacement  $u_z$ , and gives

$$u_z(a, z) = -\nu D z - \left[ \int_0^c Q_1(t) L_0^1(t, z) dt + \int_c^1 Q_2(t) L_0^1(t, z) dt \right], \quad (2.16)$$

where the kernel  $L_0^1$  reads

$$L_0^1(t, z) = \sum_n \frac{\coth(\lambda_n a) \lambda_n}{2 \cos^2 \lambda_n} P(\lambda_n, t) P(\lambda_n, z). \quad (2.17)$$

By contour integration of a suitable function in the right hand side of the complex plane<sup>4</sup>, the complex series in (2.17) can be expressed as

---

<sup>4</sup>This method has been discussed in detail in (Chatterjee and Prasad, 1973; Prasad and Chatterjee, 1973).

In any case, some details of the contour integration pertaining to (2.17) have been reported in AppendixB.

$$L_0^1(t, z) = \sum_{m=1,2,\dots}^{\infty} \frac{\sin(m\pi t) \sin(m\pi z)}{m\pi} [(m\pi a) \operatorname{cosech}^2(m\pi a) - (3 - 4\nu) \coth(m\pi a)] \\ - \sum_{m=1,2,\dots}^{\infty} \frac{\frac{2m\pi}{a^2}}{\sinh \frac{2m\pi}{a} + \frac{2m\pi}{a}} S\left(\frac{m\pi}{a}, t\right) S\left(\frac{m\pi}{a}, z\right) - (1 - \nu)^2 \frac{zt}{a}, \quad (2.18)$$

where

$$S(\lambda, t) = R(\lambda, t) + 2(1 - \nu) \frac{\sinh(\lambda t)}{\lambda}, \quad (2.19)$$

$$R(\lambda, t) = \coth \lambda \sinh(\lambda t) - t \cosh(\lambda t). \quad (2.20)$$

By using (2.16), the boundary condition (2.6) leads to the integral equation

$$\int_0^c Q_1(t) L_0^1(t, z) dt + \int_c^1 Q_2(t) L_0^1(t, z) dt = -\nu Dz, \quad 0 \leq z \leq c, \quad (2.21)$$

where  $L_0^1(t, z)$  is given by (2.18).

### 3. Solution of the elastic problem

The integral equation (2.21) needs to be re-arranged in order to be solved. The goal is to reduce it to a Fredholm equation of the second kind, which can be easily treated numerically using the properties of Jacobi polynomials.

#### 3.1. Reduction to a Fredholm equation of the second kind

It is first necessary to make the substitution

$$Q_1(z) = \frac{d}{dz} \int_z^c \frac{\theta(y)}{\sqrt{y^2 - z^2}} dy. \quad (3.1)$$

This introduces an artificial singularity in the shear stress at  $z = \pm c$ . The subsequent step will be to require that the strength of this singularity is null. By using equation (3.1) and after an integration by parts, equation (2.21) becomes

$$-\int_0^c \frac{d}{dt} L_0^1(t, z) \left[ \int_t^c \frac{\theta(y)}{\sqrt{y^2 - z^2}} dy \right] dt + \int_c^1 Q_2(t) L_0^1(t, z) dt = -\nu D z, \quad 0 \leq z \leq c. \quad (3.2)$$

The term containing  $\theta(y)$  in the equation above can be shown to be equal to

$$\begin{aligned} \int_0^c \frac{d}{dt} L_0^1(t, z) \left[ \int_t^c \frac{\theta(y)}{\sqrt{y^2 - z^2}} dy \right] dt = \\ -\frac{\pi}{2} (3 - 4\nu) \int_0^c \theta(y) \left[ \sum_{m=1,2,\dots}^{\infty} \sin(m\pi z) J_0(m\pi y) \right] dy + \frac{\pi}{2} \int_0^c \theta(y) N(y, z) dy, \end{aligned} \quad (3.3)$$

where

$$\begin{aligned} N(y, z) = \sum_{m=1,2,\dots}^{\infty} \sin(m\pi z) J_0(m\pi y) \left[ (m\pi a) \operatorname{cosech}^2(m\pi a) - (3 - 4\nu)(\coth(m\pi a) - 1) \right] \\ - \sum_{m=1,2,\dots}^{\infty} \frac{\frac{2m\pi}{a^2}}{\sinh \frac{2m\pi}{a} + \frac{2m\pi}{a}} S\left(\frac{m\pi}{a}, z\right) h_2\left(\frac{m\pi}{a}, y\right) - (1 - \nu)^2 \frac{z}{a}, \end{aligned} \quad (3.4)$$

with  $S$  given by (2.19) and  $h_2$  of the form

$$h_2(\lambda, t) = (\lambda \coth \lambda + 1 - 2\nu) I_0 - \lambda t I_1.$$

In the previous relations,  $J_0$  is the Bessel function and  $I_0$  and  $I_1$  are the modified Bessel functions (Abramowitz and Stegun (1964), Chapter 9). Making use of the following identity given in (Sneddon, 1966)

$$\sum_{m=1,2,\dots}^{\infty} \sin(m\pi z) J_0(m\pi y) = \frac{1}{\pi} \left[ \frac{H(z - y)}{\sqrt{z^2 - y^2}} - \int_0^{\infty} \exp(-s) \operatorname{cosech}(s) I_0(sy) \sinh(sz) ds \right], \quad (3.5)$$



where  $H(z - y)$  represents the Heaviside function defined as

$$H(z - y) = \begin{cases} 0, & \text{if } z - y < 0, \\ 1, & \text{if } z - y \geq 0. \end{cases} \quad (3.6)$$

The integral equation (3.2) can be written as an Abel-type equation whose solution leads to the desired Fredholm integral equation of the second kind

$$\theta(z) + z \int_0^c \theta(y) K(z, y) dy - \frac{2z}{3 - 4\nu} \int_c^1 Q_2(y) M^0(z, y) dy = -\frac{2\nu z}{3 - 4\nu} D, \quad 0 \leq z \leq c, \quad (3.7)$$

where the kernels  $K(z, y)$  and  $M^0(z, y)$  are reported in Appendix C.

In the simplest case, one may assume that the shear function  $Q_2$  is constant in the interval  $[c, 1]$ , i.e.,  $Q_2(z) = \text{const.} = q$ , so the previous relationship becomes

$$\theta(z) + z \int_0^c \theta(y) K(z, y) dy - \frac{2z}{3 - 4\nu} q \int_c^1 M^0(z, y) dy = -\frac{2\nu z}{3 - 4\nu} D, \quad 0 \leq z \leq c. \quad (3.8)$$

The integral equation (3.8) may be solved by numerical quadrature. This involves also the unknown length  $c$  that can be obtained by imposing the finiteness of stresses at the tip of the adhesive zone, or, equivalently, that the stress intensity factor  $K_{II}$  is null. The resulting condition becomes

$$K_{II} = \lim_{z \rightarrow c} 2G\sigma_{xz}(z)\sqrt{(c - z)} = 0. \quad (3.9)$$

It can be shown that, using (2.11) and (3.1), the shear stress in the adhesive zone ( $0 \leq z \leq c$ ) is given by

$$\sigma_{xz}(a, z) = (1 - \nu) \left\{ -\frac{\theta(c)z}{c\sqrt{c^2 - z^2}} + z \int_z^c \frac{d}{dt} \left[ \frac{\theta(t)}{t} \right] \frac{1}{\sqrt{t^2 - z^2}} dt \right\}. \quad (3.10)$$

Substitution of (3.10) in (3.9) leads to the condition

$$\theta(c) = 0. \quad (3.11)$$

Equations (3.8) and (3.11) constitute an eigenvalue problem for the determination of the length of the cohesive zones  $(1 - c)$  for a given set of values of  $\nu$ ,  $a$ , and provided that the cohesive stress  $q$  is known.

### 3.2. Solution of the integral equation

The integral equation (3.8) may be solved by numerical methods that exploit the properties of Jacobi polynomials. These polynomials are traditionally defined in the interval  $[-1, 1]$ , so the variables  $y$  and  $z$  are transformed as

$$y = \frac{c}{2}(t + 1), \quad 0 < y < c \quad (3.12)$$

$$z = \frac{c}{2}(s + 1), \quad 0 < z < c \quad (3.13)$$

and, accordingly,  $\theta(y) = \theta_1(t)$ . The integral equation thus reads

$$\theta_1(s) + \frac{c^2}{4}(s + 1) \int_{-1}^1 \theta_1(t) K(s, t) dt = \frac{c(s + 1)}{3 - 4\nu} [q F(s, c) - \nu D], \quad (3.14)$$

where  $F(s, c)$  has been reported in AppendixC. The discretized form of the integral equation can be therefore obtained by employing the Gauss-Jacobi quadrature formula

$$\theta_1(s_j) + \frac{c^2}{4}(s_j + 1) \sum_{i=1}^{n_1} w_i^{(0,0)} \theta_1(t_i) K(s_j, t_i) = \frac{c(s_j + 1)}{3 - 4\nu} [q F(s_j, c) - \nu D], \quad j = 1, \dots, n_1, \quad (3.15)$$

where, from (2.13), one can write

$$D = \frac{\Delta}{a} - \frac{\pi\nu c}{4a} \sum_{i=1}^{n_1} w_i^{(0,0)} \theta_1(t_i) + \frac{\nu(1-c^2)}{a} q, \quad (3.16)$$

with  $\Delta$  assumedly known.

The integration points  $t_i$

$$P_{n_1}^{(0,0)}(t_i) = 0, \quad i = 1, \dots, n_1, \quad (3.17)$$

represent the roots of the Jacobi polynomials of the first kind  $P_n^{(\alpha,\beta)}(t)$  ( $\alpha = \beta = 0$  for the case at hand), which coincide with the Legendre polynomials of the first kind  $P_n(t)$ , while  $w_i^{(\alpha,\beta)}$  represent the correspondent weights of Jacobi integration formula. The collocation points  $s_i$  ( $i = 1, \dots, n_1$ ) are chosen to be coincident with the integration points, i.e.,  $s_i = t_i$ . Equation (3.14) provides a system of  $n_1$  equations in  $n_1 + 1$  unknowns. The condition

$$\theta_1(1) = 0, \quad (3.18)$$

which satisfies (3.11), must also be fulfilled to obtain  $c$  as a part of the solution.

Displacements and stresses may be evaluated through equations (2.8) and (2.10), by employing (2.14) for  $A_n$ . In particular, the following expression may be obtained for the contact normal stress  $\sigma_{xx}(a, z)$

$$\begin{aligned} \sigma_{xx}(a, z) = D + \frac{1-2\nu}{2} \left[ \theta'(z) + \int_0^z \frac{y[\theta'(y) - \theta'(z)]}{z\sqrt{z^2 - y^2}} dy \right] + \int_0^c \theta(y) L^1(y, z) dy \\ - q \left[ \frac{1-2\nu}{\pi} \int_c^1 \frac{y}{y^2 - z^2} dy - \int_c^1 L^2(y, z) dy \right], \quad 0 \leq z \leq c, \quad (3.19a) \end{aligned}$$

$$\sigma_{xx}(a, z) = D - \frac{1-2\nu}{2} \int_0^c \theta(y) \frac{z}{(z^2 - y^2)^{3/2}} dy + \int_0^c \theta(y) L^1(y, z) dy + q H(c, z), \quad c \leq z \leq 1, \quad (3.19b)$$

where  $L^1(y, z)$ ,  $L^2(y, z)$  and  $H(c, z)$  are collected in AppendixC.

#### 4. Numerical results

The solution of the problem of Figure 4 is the sum of the contribution of the two subproblems of Sections 2.1 and 2.2. The state of stress is given by

$$\sigma_{xx}^{tot}(a, z) = \sigma_{xx}^I(a, z) + \sigma_{xx}^{II}(a, z) = -p_T + \sigma_{xx}(a, z), \quad (4.1)$$

$$\sigma_{xz}^{tot}(a, z) = \sigma_{xz}^I(a, z) + \sigma_{xz}^{II}(a, z) = \sigma_{xz}(a, z), \quad (4.2)$$

where  $\sigma_{xz}$  and  $\sigma_{xx}$  are given by equations (3.10) and (3.19), respectively.

The problem is completely described by the following parameters: Poisson's ratio  $\nu$ , aspect ratio  $a$ , thermal deformation  $\varepsilon_T$ , and the cohesive stress  $q$ . The cohesive zone length  $(1 - c)$  can be obtained as a solution of the problem once these parameters are fixed.

In order to obtain numerical results, it is important to determine first the expression of the term  $D$  of equation (3.15). From (2.10a) and (A.9), it is clear that

$$p_T b = h \int_{-1}^1 2G\sigma_{xx}(a, z) dz = 4GhD, \quad (4.3)$$

and, recalling that  $p_T 2h = \frac{E\varepsilon_T}{\nu(1+\nu)} 2h$ , one has

$$D = \frac{\varepsilon_T}{\nu}. \quad (4.4)$$

From (3.16), one can also determine the displacement  $\Delta$  as

$$\Delta = \frac{\varepsilon_T a}{\nu} + \frac{\pi\nu}{2} \int_0^c \theta(t) dt - \frac{\nu q}{2} (1 - c^2). \quad (4.5)$$

In order to present the results, recall that the strain  $\varepsilon_T$  is associated with a thermal mismatch between the rectangle and the plates and is of the form

$$\varepsilon_T = \alpha^* \Delta T = (\alpha_r - \alpha_p) \Delta T, \quad (4.6)$$

where  $\alpha_p$  and  $\alpha_r$  represent the coefficient of thermal expansion of plates and rectangle, respectively, and  $\Delta T$  is the temperature variation.

#### 4.1. The response of “soft” joints

The dependence of the cohesive length upon the various parameters is shown in Figure 5. In particular, Figure 5(a) shows the trend of the normalized length<sup>5</sup> of the cohesive zone  $(1 - c)/a$  as a function of the aspect ratio  $a$ , for different values of the Poisson’s ratio  $\nu$  ( $\nu = 0.1 \div 0.5$ ). Such curves correspond to the case of a *soft* joint, characterized by a low Young’s modulus  $E = 1$  MPa, with thermal parameters  $\alpha_p = 10.5 \cdot 10^{-6} \text{ C}^{-1}$ ,  $\alpha_r = 290 \cdot 10^{-6} \text{ C}^{-1}$ ,  $\Delta T = 20^\circ\text{C}$ , and  $q = 0.8 \text{ MPa}/2G$ .

Clearly, the cohesive zone tends to decrease as the aspect ratio  $a$  increases, tending to zero as  $a \rightarrow \infty$ . Such a trend is the more accentuated, the higher the value of Poisson’s ratio is. A thermal mismatch can therefore be critical when dealing with long bonded joints that, for fixed thickness of the adhesive, correspond to low aspect ratios<sup>6</sup>. One should also notice that the widest cohesive zones are obtained for incompressible materials ( $\nu \rightarrow 0.5$ ), while the curves tend to flatten for materials with negligible lateral contraction, as evident in Figure 5(a).

Figure 5(b) shows the variation of the cohesive length with the aspect ratio  $a$  when different temperature gradients are considered, namely from  $\Delta T = 20^\circ\text{C}$  to  $\Delta T = 100^\circ\text{C}$ , for fixed  $\nu = 0.5$  and  $q = 0.8 \text{ [MPa]}/2G$ . The size of the cohesive zone increases at high temperature

<sup>5</sup>The length of the cohesive zone is  $[(1 - c)/a]H/2$ .

<sup>6</sup>Due to numerical instabilities, aspect ratios lower than  $a = 0.075$  have not been considered.

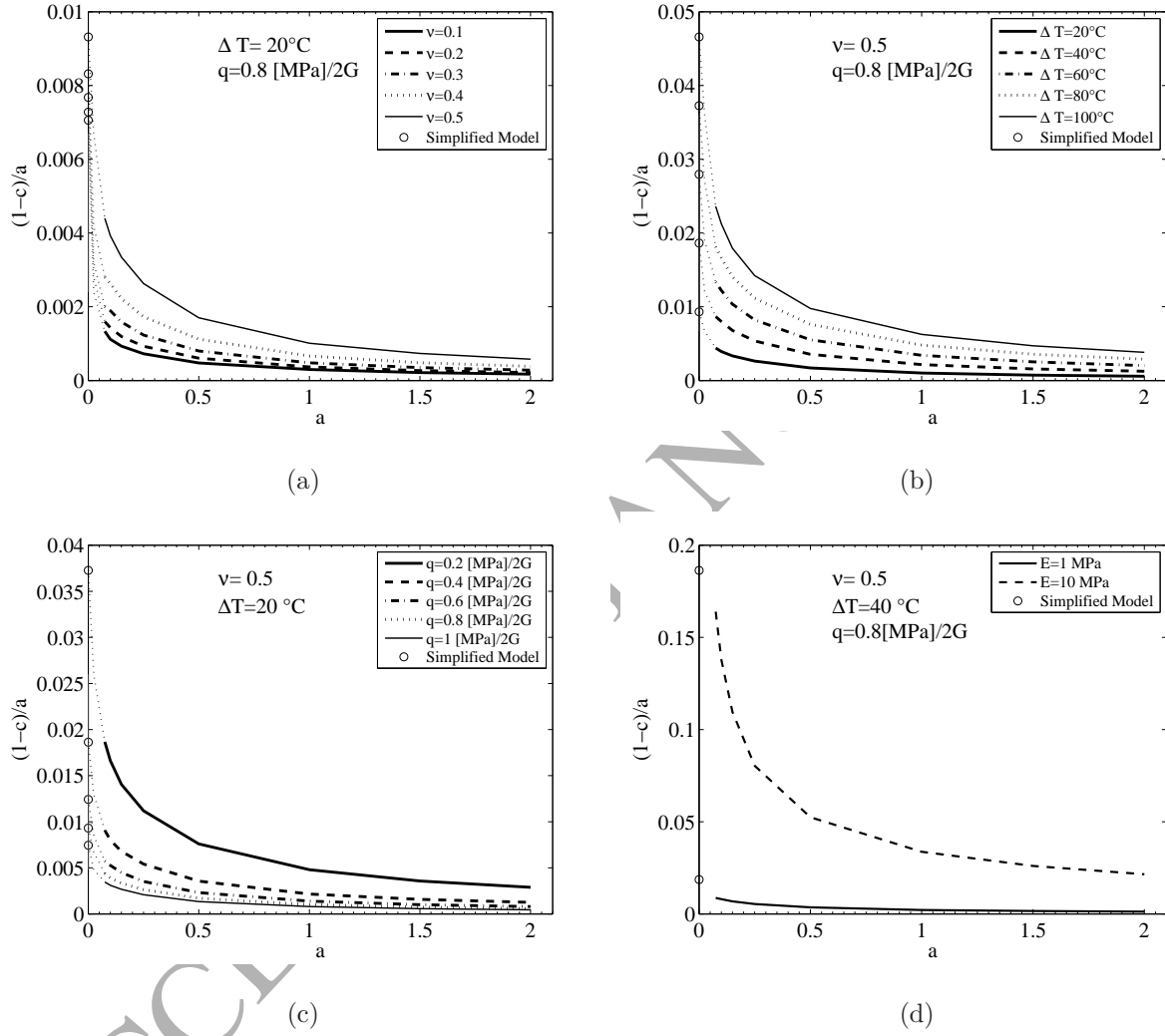


Figure 5: Normalized cohesive zone length  $(1-c)/a$  as a function of the aspect ratio  $a$ . a) Influence of the Poisson's ratio  $\nu$ ; b) influence of the temperature variation  $\Delta T$ ; c) influence of the cohesive shear stress  $q$ ; d) influence of the Young's modulus  $E$ .

variations and for low aspect ratios. For the sake of comparison, the results from the elementary model evaluated through (1.1) are reported in the same figure on the axis  $a = 0$  and evidenced with a circle marker. Quite interestingly, such estimates represent an upper bound for the size of the cohesive zone. In other words, the elementary approach gives reliable results only when the width of the bonded joint tends to infinite or, equivalently, its thickness tends to zero. Moreover, the curves obtained for different temperature gradients tend to the value predicted by the simplified model as  $a \rightarrow 0$ : their dotted extension indicates this trend.

Regarding the effect of the cohesive shear stress  $q$ , it is clear from Figure 5(c) that increasing  $q$  the cohesive length decreases (graphs corresponding to  $\nu = 0.5$  and  $\Delta T = 20^\circ\text{C}$ ). The same figure reports also the results of the elementary model (equation (1.1) for varying  $q$ ), again evidenced by circle markers at  $a = 0$ , which represent the asymptotic limit of the various curves (dashed extensions).

It is well known (Ward and Sweeney, 2005; Hooper, 1964) that the mechanical properties of polymers are greatly affected by temperature and that they tend to stiffen at very low temperatures. Hooper (1964), for example, observed that silicones are very low in rigidity at room temperature and stiffen very slowly if the temperature is diminished, but below a certain limit ( $-16^\circ\text{C}$  for a 40 Shore-A silicone) the stiffness starts to increase very rapidly and a 10 times higher elastic modulus can be reached at  $-20^\circ\text{C}$ . Therefore, it is interesting to observe the variation of the cohesive length when the Young's modulus is increased. In Figure 5(d) two graphs are juxtaposed, associated with different values of the Young's modulus, one ten times higher than the other, and for  $\Delta T = 40^\circ\text{C}$ . There is a noteworthy enlargement of the cohesive zone for stiff adhesives, and of course the increase is more evident for low aspect ratios. The circle markers again indicate results from the elementary approach as *per* (1.1). Apparently, one could deduce that the simplified model is accurate (in the limit  $a \rightarrow 0$ ) for a low stiffness, but the accuracy is lost when the Young's modulus is increased. In fact, the corresponding point does not connect with the asymptotic limit of the graph, remaining much lower than expected. However, it will be shown more in detail in Section

4.2 that this is not exactly the case.

It is also of interest to analyze the distribution of contact stresses at the interface for different values of the aspect ratio  $a$ . Figure 6 represents the interfacial shear stress deduced from (3.10) as a function of the coordinate  $z$ , for fixed  $\Delta T$  and  $q$  (only half-width of the rectangle is plotted thanks to symmetry). In this case, to evidence the dependence by  $a$ , the joint width  $b$  has been maintained fixed while the height  $H$  has been varied. The graphs show that the stress presents peaks in the cohesive zones, and then rapidly decreases. The stress is continuous but it kinks at the frontier point between the adhesive and the cohesive zone, where the shear stress is constant. The higher shear stress is associated with the lower values of  $a$ , but the difference is minimal because all the curves tend to overlap. The normal stress at the interface, evaluated through (3.19) and represented in Figure 6(b), shows a similar trend: the stress is almost null for most part of the width, except in a small zone near the extremity of the rectangle. In this case, the milder stress distributions correspond to the higher aspect ratios, but the difference is not remarkable.

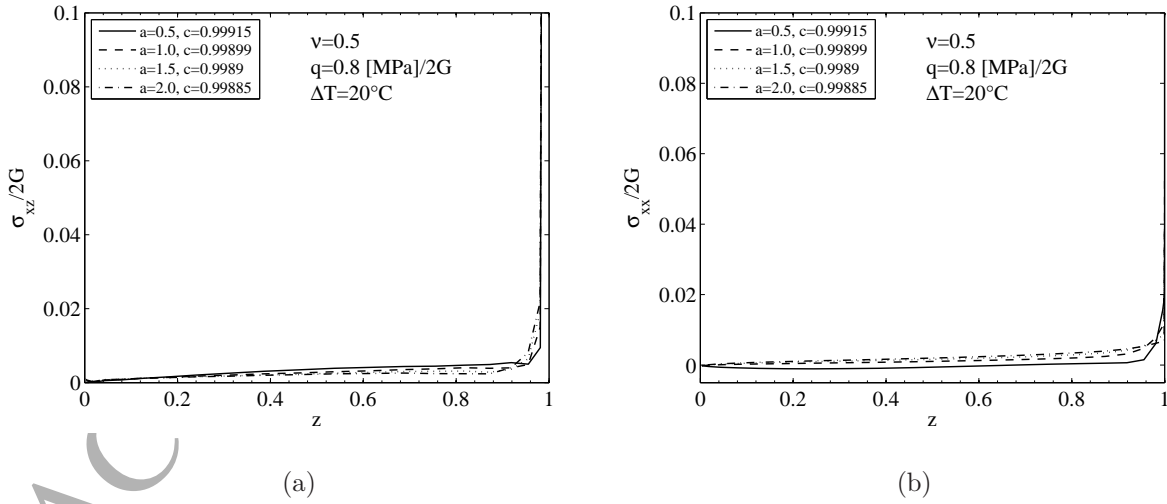


Figure 6: Distribution of contact shear stress  $\sigma_{xz}$  and normal stress  $\sigma_{xx}$  for different values of the aspect ratio  $a$  ( $b = \text{const.}$  and  $H$  variable).



#### 4.2. The behavior of “stiff” joints

In the previous section it has been observed that by changing the stiffness of the adhesive, the size of the cohesive zone varies as well. To further illustrate this point, the graphs of Figure 7 show the normalized cohesive zone length  $(1 - c)/a$  as a function of the aspect ratio  $a$ , for different values of the Young’s modulus  $E$  of the adhesive layer. Obviously, there is a limit condition associated with the geometry of the problem, dictated by the fact that the size of the cohesive zone cannot be larger than the width of the whole bonded joint. Such a limit case is associated with the curve represented by the thickest line. Figure 7(b) and Figure 7(c) represent the same graphs of Figure 7(a), but in semi-logarithmic and bi-logarithmic scale, respectively, in order to appreciate the trend of the cohesive zone length for very soft joints, hardly visible otherwise.

It should be observed that, keeping fixed the elastic modulus, the curves asymptotically tend to the limit curve when the parameter  $a$  increases, that is, when the joint is thick with respect to its width. This means that the interface becomes completely cohesive and the joint is completely yielded. In fact, strong cohesive forces are needed to stretch the joint and accommodate the thermal expansion when the overall stiffness of the adhesive layer increases, i.e., when its height is augmented. This trend is the more marked the stiffer the joint is (high Young’s modulus). In fact, in stiff joints the deformation is of the kind qualitatively represented in Figure 8(a): the external *lamellae* tend to deform, but the interlayer is so stiff that the only way to comply with such a deformation is to develop a wide cohesive zone. On the other hand, as schematically illustrated in Figure 8(b), in “soft” joints the elastic deformation is able to accommodate most of the thermal dilatation of the external plies, without the need of developing a marked cohesive zone.

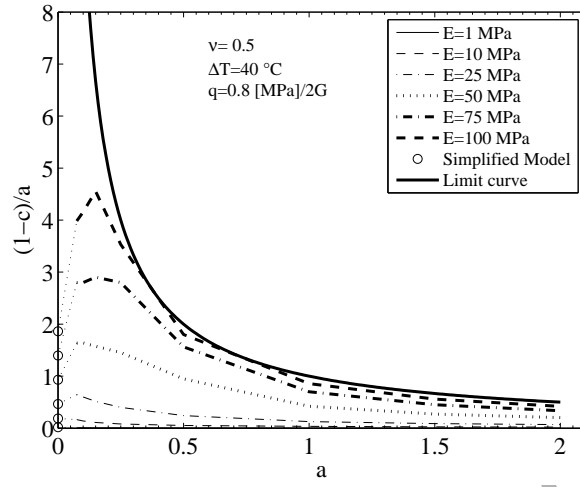
For what concerns the left-hand-side part of the graphs, when  $a \rightarrow 0$ , the response is more complex. For any  $E$ , as indicated by the dashed extensions of the graphs, the size of the cohesive zone tends to the values predicted by the simplified model of equation (1.1), evidenced by the circles at  $a = 0$ . When  $E$  is sufficiently high, the parameter  $c$  tends to become close to 1, but a maximum value is reached for  $a \simeq 0.25$  and then the cohesive length

tends to diminish when  $a \rightarrow 0$ . On the contrary, when the joint is soft (low values of  $E$ ), the cohesive zone is always a decreasing function of  $a$ . This behavior can be explained by observing that the external plies induce a confining action. In very soft joints, the confining effect is noteworthy, so that the wider the bonded joint is, its height fixed (or, equivalently, the thinner the joint, its width fixed), the higher the cohesive length is. In stiff joints, there is a competition between the stiffness of the joint itself and the confining action of the external plies. The confining action is the most effective for a certain aspect ratio ( $a \simeq 0.25$ ), below which no further increase of the cohesive length is evidenced. In other words, decreasing the aspect ratio of the bonded joint does not always correspond to an increase of the cohesive length.

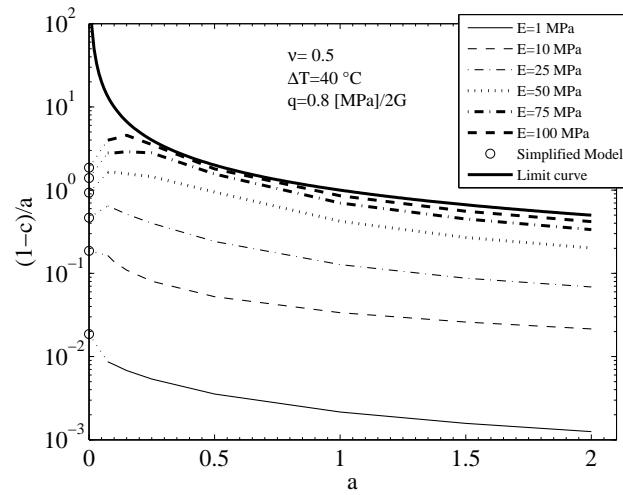
One can thus also explain the *apparently* anomalous response of Figure 5(d), where it was mentioned that the graph corresponding to the higher Young's modulus did not tend, in the limit  $a \rightarrow 0$ , to the point corresponding to the simplified model of (1.1). In fact, for the specific case there considered, numerical instabilities prevented to recognize the aspect ratio corresponding to the maximal extension of the cohesive zone, which is instead clear in the graphs of Figure 7 for the stiff joints.

It can also be interesting to analyze the distribution of contact stresses at the interface for different values of the aspect ratio  $a$  when the joint is "stiff" ( $E = 100$  MPa). Figure 9(a) represents the interfacial shear stress as a function of the coordinate  $z$  (see Figure 3), for fixed  $\Delta T$  and  $q$ . First of all, observe that much larger cohesive zones are obtained if one compares such a graph with that corresponding to a "soft" joint (Figure 6(a) for  $E = 1$  MPa). The stress increases in the adhesive portions and matches with the constant value, characteristic of the cohesive zone. In general, the cohesive length increases as the aspect ratio increases (thicker joints) but an inversion of this trend is evidenced for very high values of the aspect ratio  $a$ .

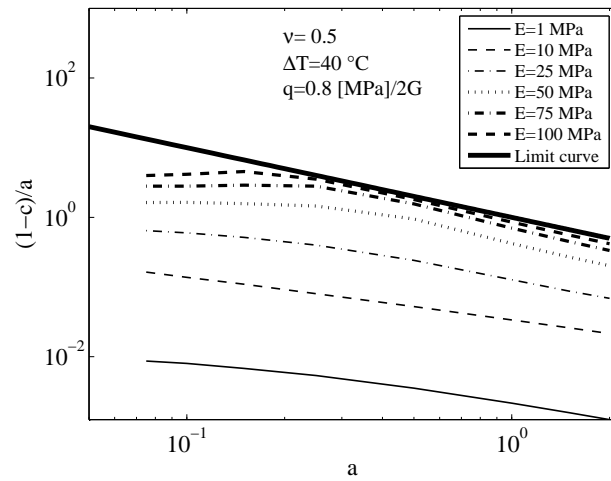
The normal stress at the interface, represented in Figure 9(b), shows another interesting trend. For low aspect ratios, there is a sign inversion along the bond length while, for high aspect ratios, the stress is almost null in most part of the bonded length, reaching the



(a)



(b)



(c)

Figure 7: Cohesive zone length  $(1-c)/a$  as a function of the aspect ratio  $a$ . Influence of the Young's modulus  $E$  and of the aspect ratio  $a$ . Graph in a) linear scale; b) semi-logarithmic scale; c) bi-logarithmic scale.

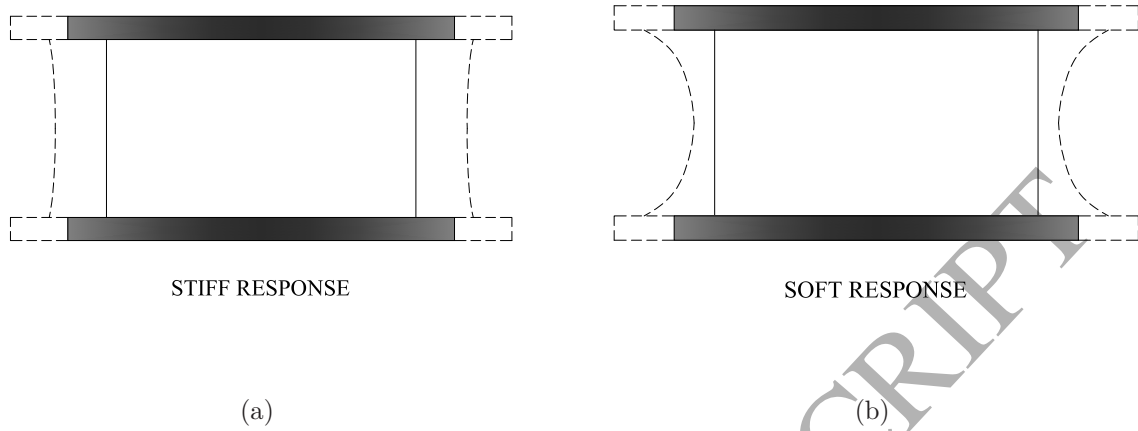


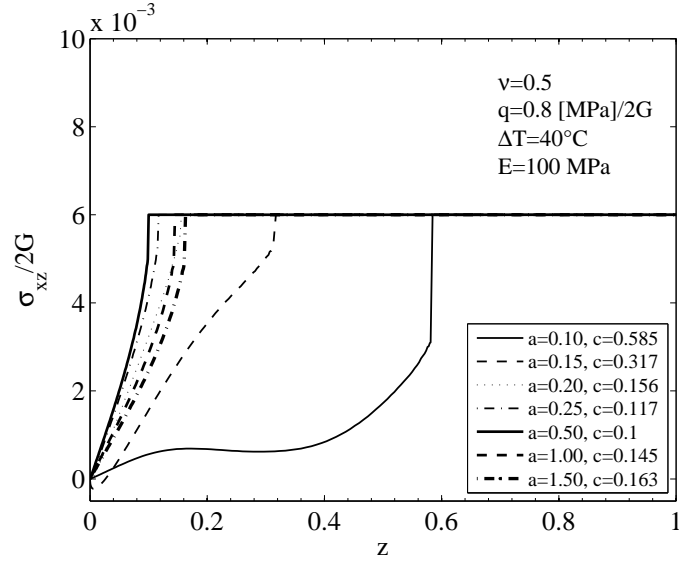
Figure 8: Qualitative response of a bonded joint: a) “stiff” joint; b) “soft” joint.

maximum values at the borders of the rectangle.

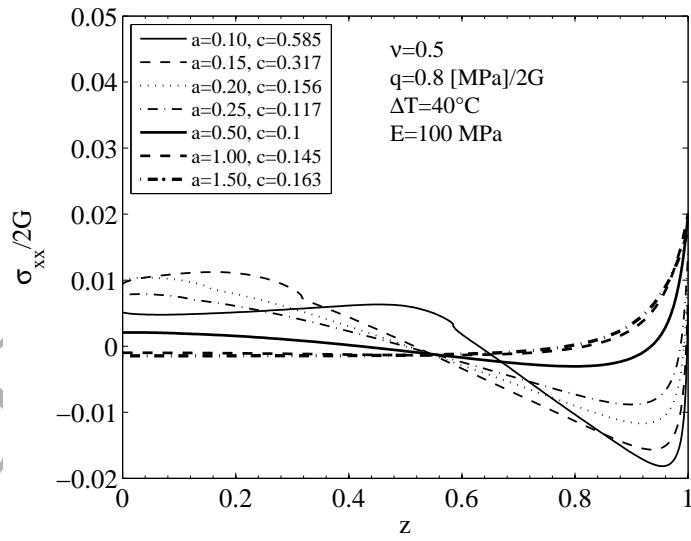
## 5. Discussion and conclusions

Adhesive joints are increasingly being used to provide the structural bond of different in type materials. This technique is simple and effective, but problems can arise while bonding materials with different coefficients of thermal expansion, because of their different expansion/contraction. This is the reason why most technical guidelines recommend to use adhesive layers thick enough to compensate, with their compliance, the thermal mismatch of the adherends. However, the deformation of the adhesive material itself, although presenting a coefficient of thermal expansion orders of magnitude greater than that of the adherends, is usually neglected. The aim of this work consists in clarifying this effect.

The model problem considered here is that of an elastic rectangle in plane strain, representative of the adhesive layer, sandwiched by two external plates, representing the adherends. Adhesive and adherends have different coefficient of thermal expansion and we suppose that their interface is characterized by a step-wise shear-stress vs. slip constitutive law, which represents a first-order approximation of more complicated cohesive laws that have been proposed in the literature according to experimental results.



(a)



(b)

Figure 9: Distribution of contact shear stress ( $\sigma_{xz}$ ) and normal stress ( $\sigma_{xx}$ ) for different values of the aspect ratio  $a$  for a stiff adhesive joint with  $E = 100$  MPa ( $b = \text{const.}$  and  $H$  variable).

A very simple and practical way to analyze the effects produced by temperature variations is to suppose that the state of stress in the elastic rectangle is uniform and uniaxial. It is then very easy to obtain an explicit characterization of the size and location of the *cohesive* zones, where the shear-stress limit is attained at the price of a relative slip between adhesive and adherend, and of the *adhesive* zones, where the bond is perfect. The contact shear-stress deforms the elastic adhesive layer so to counterbalance the thermal strain induced by the thermal variation. In this elementary approach, the state of stress does not depend upon the width of the joint but only upon its height.

A more refined analysis has been conducted by considering in detail the elastic deformation of the rectangle. This is a contact problem in linear elasticity theory. The contact area between adhesive and adherend is formed by an adhesive zone surrounded by cohesive regions, where the shear stress is known and assumed constant according to the accredited interface law. In order to satisfy the boundary conditions on the free borders of the elastic rectangle, the solution is found in terms of Papkovitch-Fadle eigenfunctions. The contact is governed by an integral equation whose solutions have been obtained by employing the Jacobi integration formula, exploiting the properties of Jacobi polynomials. The size of the cohesive zone can be determined by imposing the zeroing of the stress intensity factor at the frontier between the cohesive and the adhesive zones.

The results evidence that the size of the cohesive zone depends upon parameters that have no influence in the aforementioned elementary approach, in particular the aspect ratio of the adhesive joint, defined as the ratio between the height and the width of the adhesive layer. Of course, the higher the temperature variation, the wider is the cohesive zone, and such a dependence is more marked for low aspect ratios. On the other hand, an increase of the limit shear stress in the interface constitutive law diminishes the length of the cohesive zone, and again this effect is higher for low aspect ratios.

In general, supposed fixed the height of the joint, the length of the cohesive zone diminishes as the width of the joint is reduced (high aspect ratio). On the other hand, an increase of the cohesive zone is evident when considering low aspect ratios, i.e., under equal conditions

adhesive rupture is likely to happen in wide bonded joints. The Poisson's ratio of the material has an effect for low aspect ratios, while its influence became less evident for low values of the width (high aspect ratio) because, for such a geometry, the confining effect of the plates is limited.

Remarkably, a distinction should be made between “stiff” and “soft” joints, especially for wide joints, whose response is strongly affected by the material elastic modulus. Obviously, the stiffer the joint, the wider is the cohesive zone, because the elastic deformation of the material becomes less capable of accommodating the differential thermal expansion, and the interface consequently yields. What is more, in *soft* joints the size of the cohesive zone is a monotone decreasing function of the aspect ratio, while in *stiff* joints there is a critical value of the aspect ratio that corresponds to the maximal extension of the cohesive zone. This effect has been attributed to the competition between the confining effect of the contouring plates and the stiffness of the joint itself. It is interesting to notice that, in all cases, as the aspect ratio tends to zero (very wide joints), the size of the cohesive zone tends to the value predicted by the elementary approach mentioned above. Therefore, such a value is an upper bound for soft joints only, whereas for stiff joints the elementary model does not furnish any indication either about the extension of the cohesive zone, or about the critical aspect ratio.

For what concerns the interface stresses, the maximum shear stress is concentrated in the cohesive zone and rapidly diminishes outside of that. This decay is the more evident the lower is the elastic modulus of the material and, in general, there is also a dependence upon the aspect ratio. The normal component of stress at the interface must have zero resultant and, consequently, it is formed by alternating zones of tension and compressions. Also in this case, the result depends upon the aspect ratio and the stiffness of the adhesive layer.

In conclusion, we have evidenced the influence of various competing parameters, such as the stiffness of the material, the limit cohesive shear stress at the interface and the aspect ratio of the joint itself. It should be recalled that a temperature variation can produce not only a deformation, but can also affect the elastic modulus and the limit shear stress of

the adhesive. For example, in silicone sealants low temperatures can cause an increase of the elastic modulus of one order of magnitude with respect to room temperature, and the cohesive limit stress tends to diminish. Therefore, a detailed study seems to be necessary especially when the height of the joint is not negligible with respect to its width, as it is the rule when bonding dissimilar adherends.

Of course, the study proposed here is far from being exhaustive. An extensive experimental campaign is certainly necessary to corroborate the theoretical conclusions. In any case, this article has contributed to raise questions about the reliability of existing design rules in predicting the height of a bonded joint, to accommodate the thermal variations that it undergoes during its lifetime. The study has also evidenced the influence of the various parameters that play a significant role in the phenomenon, most of which are usually neglected in the design practice.

**Acknowledgements.** The authors acknowledge for partial support the European Community under contract RFSR-CT-2012-00026 (S+G RFS-PR-11017).

## Appendix A. Papkovitch-Fadle eigenfunction solutions

The solution of the differential equations

$$2(1 - \nu)\nabla^2\Omega + \frac{\partial^2\Psi}{\partial z^2} = 0, \quad (\text{A.1a})$$

$$\nabla^2\Psi = 0, \quad (\text{A.1b})$$

with  $\nu$  Poisson's ratio and  $\nabla^2 = \frac{\partial^2}{\partial x^2} + \frac{\partial^2}{\partial z^2}$ , is expanded in the form

$$\Omega(x, z) = \frac{D}{2} [(1 - \nu)x^2 - (2 - \nu)z^2] - \sum_{n=-\infty}^{\infty} A_n \cosh(\lambda_n x) f_{1n}(z), \quad (\text{A.2a})$$

$$\Psi(x, z) = D(1 - \nu)(z^2 - x^2) - 2(1 - \nu) \sum_{n=-\infty}^{\infty} A_n \cosh(\lambda_n x) f_{2n}(z), \quad (\text{A.2b})$$



where  $A_n$  are unknown complex constants and  $f_{1n}$  and  $f_{2n}$  constitute a set of complex valued eigenfunctions satisfying the following differential equations:

$$f_{1n}'' + \lambda_n^2 f_{1n} = \lambda_n^2 f_{2n}, \quad (\text{A.3a})$$

$$f_{2n}'' + \lambda_n^2 f_{2n} = 0, \quad (\text{A.3b})$$

with the boundary conditions

$$(1 - \nu) f_{2n}(\pm 1) + f_{1n}(\pm 1) = 0, \quad (\text{A.4a})$$

$$(1 - \nu) f_{2n}'(\pm 1) + f_{1n}'(\pm 1) = 0, \quad (\text{A.4b})$$

where  $f' = df/dz$  and  $\lambda_n$  are the nonzero complex roots of the equation

$$\sin 2\lambda_n + 2\lambda_n = 0. \quad (\text{A.5})$$

The set of complex valued Papkovitch-Fadle eigenfunctions  $f_{1n}$  and  $f_{2n}$ , whose expressions are given by

$$\begin{aligned} f_{1n}(z) &= [\lambda_n \tan \lambda_n + 2(1 - \nu)] \cos(\lambda_n z) - \lambda_n z \sin(\lambda_n z), \\ f_{2n}(z) &= -2 \cos(\lambda_n z), \end{aligned} \quad (\text{A.6})$$

is associated with the set of functions  $g_{1k}$  and  $g_{2k}$  as per

$$\begin{aligned} g_{1k}(z) &= \frac{1}{4 \cos^2(\bar{\lambda}_k)} \left\{ - [\bar{\lambda}_k \tan \bar{\lambda}_k + 2\nu] \cos(\bar{\lambda}_k z) + \bar{\lambda}_k z \sin(\bar{\lambda}_k z) \right\}, \\ g_{2k}(z) &= -\frac{2 \cos(\bar{\lambda}_k z)}{4 \cos^2(\bar{\lambda}_k)}, \end{aligned} \quad (\text{A.7})$$

where  $\overline{(\cdot)}$  is the complex conjugation, so to fulfill the orthonormality condition

$$\int_{-1}^1 \left[ f_{1n}(z) \overline{g_{2k}(z)} + f_{2n}(z) \overline{g_{1k}(z)} \right] dz = \begin{cases} 0, & \text{for } k \neq n, \\ 1, & \text{for } k = n. \end{cases} \quad (\text{A.8})$$

Moreover, it can be verified that the following condition also holds

$$\int_{-1}^1 [\nu f_{2n}(z) - f_{1n}(z)] dz = 0. \quad (\text{A.9})$$

The stresses  $\sigma_{xx}$ ,  $\sigma_{zz}$  and  $\sigma_{xz}$  can be expressed, in terms of  $\Omega$  and  $\Psi$ , in the form

$$\frac{\sigma_{xx}}{2G} = \frac{\nu}{2(1-\nu)} \frac{\partial^2 \Psi}{\partial z^2} + \frac{\partial^2 \Omega}{\partial x^2}, \quad (\text{A.10a})$$

$$\frac{\sigma_{zz}}{2G} = \frac{\nu}{2(1-\nu)} \frac{\partial^2 \Psi}{\partial z^2} + \frac{\partial^2}{\partial z^2} (\Psi + \Omega), \quad (\text{A.10b})$$

$$\frac{\sigma_{xz}}{2G} = \frac{\partial^2 (2\Omega + \Psi)}{2\partial x \partial z}, \quad (\text{A.10c})$$

whereas for the displacements one finds

$$u_x = \frac{\partial \Omega}{\partial x}, \quad (\text{A.11a})$$

$$u_z = \frac{\partial}{\partial z} (\Omega + \Psi). \quad (\text{A.11b})$$

## Appendix B. Contour integration

In order to reduce (2.17) to a real form, consider the integration of the function

$$\frac{\xi \coth(\xi a)}{\sin 2\xi + 2\xi} P(\xi, t) P(\xi, z), \quad (\text{B.1})$$

around the contour  $\Gamma$  consisting of the imaginary axis with indentations around the points  $\xi = \frac{im\pi}{a}$ , the semicircle  $|\xi| = (N + 1/2)\pi$  in the right hand half plane and the circles around the points  $\xi = \lambda_n$  ( $n = -N, \dots, -1, 1, \dots, N$ ) as well as  $\xi = m\pi$  ( $m = 1, \dots, N$ ).

The residues of the function at the points  $\xi = \lambda_n$ ,  $\xi = m\pi$ ,  $\xi = im\pi/a$  and  $\xi = 0$  are

$$\xi = \lambda_n \rightarrow \frac{\lambda_n \coth(\lambda_n a)}{4 \cos^2 \lambda_n} P(\lambda_n, t)(\lambda_n, z), \quad (\text{B.2})$$

$$\xi = m\pi \rightarrow -\frac{\sin(m\pi t) \sin(m\pi z)}{2m\pi} [(m\pi a) \operatorname{cosech}^2(m\pi a) - (3 - 4\nu) \coth(m\pi a)], \quad (\text{B.3})$$

$$\xi = 0 \rightarrow (1 - \nu)^2 \frac{tz}{a}, \quad (\text{B.4})$$

$$\xi = \frac{im\pi}{a} \rightarrow \frac{\frac{\eta}{a}}{\sinh 2\eta + 2\eta} S(\eta, t) S(\eta, z), \quad (\text{B.5})$$

where

$$\begin{aligned} \eta &= \frac{m\pi}{a}, \\ S(\eta, t) &= R(\eta, t) + 2(1 - \nu) \frac{\sinh(\eta t)}{\eta}, \\ R(\eta, t) &= \coth \eta \sinh(\eta t) - t \cosh(\eta t). \end{aligned}$$

By applying the Residue Theorem, one obtains

$$\begin{aligned} \sum_{n=-\infty}^{\infty} \frac{\lambda_n \coth(\lambda_n a)}{2 \cos^2 \lambda_n} P(\lambda_n, t)(\lambda_n, z) = \\ \sum_{m=1,2,\dots}^{\infty} \frac{\sin(m\pi t) \sin(m\pi z)}{m\pi} [(m\pi a) \operatorname{cosech}^2(m\pi a) - (3 - 4\nu) \coth(m\pi a)] \\ - \sum_{m=1,2,\dots}^{\infty} \frac{\frac{2m\pi}{a^2}}{\sinh \frac{2m\pi}{a} + \frac{2m\pi}{a}} S\left(\frac{m\pi}{a}, t\right) S\left(\frac{m\pi}{a}, z\right) - (1 - \nu)^2 \frac{tz}{a}, \quad (\text{B.6}) \end{aligned}$$

which coincides with equation (2.18).

## Appendix C. Kernels

Here is a list of the expressions of the kernels that are used throughout this article.

$$K(z, y) = -K_1(z, y) + K_2(z, y) + K_3(z, y) + K_4(z, y), \quad (\text{C.1})$$

with

$$\begin{aligned} K_1(z, y) &= \int_0^\infty s \exp(-s) \operatorname{cosech} s I_0(sy) I_0(sz) ds, \\ K_2(z, y) &= \frac{\pi^2}{3-4\nu} \sum_{m=1,2,\dots}^\infty m J_0(m\pi y) J_0(m\pi z) \left[ -(m\pi a) \operatorname{cosech}^2(m\pi a) + (3-4\nu)(\coth(m\pi a) - 1) \right], \\ K_3(z, y) &= \frac{\pi}{3-4\nu} \sum_{m=1,2,\dots}^\infty \frac{\frac{2m\pi}{a^2}}{\sinh \frac{2m\pi}{a} + \frac{2m\pi}{a}} h_2\left(\frac{m\pi}{a}, z\right) h_2\left(\frac{m\pi}{a}, y\right), \\ K_4(z, y) &= \frac{\pi}{3-4\nu} \frac{(1-\nu)^2}{a}. \end{aligned}$$

$$M^0(y, z) = M_1^0(y, z) - M_2^0(y, z) + M_3^0(y, z) + M_4^0(y, z), \quad (\text{C.2})$$

with

$$\begin{aligned} M_1^0(y, z) &= \frac{3-4\nu}{\pi} \left[ \frac{H(y-z)}{\sqrt{y^2-z^2}} \int_0^\infty \exp(-s) \operatorname{cosech} s I_0(sz) \sinh(sy) ds \right], \\ M_2^0(y, z) &= \sum_{m=1,2,\dots}^\infty \sin(m\pi y) J_0(m\pi z) \left[ (m\pi a) \operatorname{cosech}^2(m\pi a) - (3-4\nu)(\coth(m\pi a) - 1) \right], \\ M_3^0(y, z) &= \sum_{m=1,2,\dots}^\infty \frac{\frac{2m\pi}{a^2}}{\sinh \frac{2m\pi}{a} + \frac{2m\pi}{a}} S\left(\frac{m\pi}{a}, y\right) h_2\left(\frac{m\pi}{a}, z\right), \\ M_4^0(y, z) &= \frac{(1-\nu)^2}{a} y. \end{aligned}$$

$$F(c, z) = \int_c^1 M^0(y, z) dy = F_1(c, z) - F_2(c, z) + F_3(c, z) + F_4(c, z), \quad (\text{C.3})$$

with

$$\begin{aligned}
 F_1(c, z) &= \frac{3-4\nu}{\pi} \left[ \log \frac{1+\sqrt{1-z^2}}{c+\sqrt{c^2-z^2}} - \int_0^\infty \exp(-s) \operatorname{cosech} s I_0(sz) \frac{\cosh(s) - \cosh(sc)}{s} ds \right], \\
 F_2(c, z) &= \sum_{m=1,2,\dots}^\infty \frac{\cos(m\pi c) - \cos(m\pi)}{m\pi} J_0(m\pi z) [(m\pi a) \operatorname{cosech}^2(m\pi a) - (3-4\nu)(\coth(m\pi a) - 1)], \\
 F_3(c, z) &= \sum_{m=1,2,\dots}^\infty \frac{\frac{2m\pi}{a^2}}{\sinh \frac{2m\pi}{a} + \frac{2m\pi}{a}} h_3\left(\frac{m\pi}{a}, c\right) h_2\left(\frac{m\pi}{a}, z\right), \\
 F_4(c, z) &= \frac{(1-\nu)^2}{a} \frac{1-c^2}{2}.
 \end{aligned}$$

$$L^1(y, z) = -L_1^1(y, z) - L_2^1(y, z) + L_3^1(y, z), \quad (\text{C.4})$$

with

$$\begin{aligned}
 L_1^1(y, z) &= \frac{1-2\nu}{2} \left[ \int_0^\infty s \exp(-s) \operatorname{cosech} s I_0(sy) \cosh(sz) ds \right], \\
 L_2^1(y, z) &= \frac{\pi}{2} \sum_{m=1,2,\dots}^\infty m\pi \cos(m\pi z) J_0(m\pi y) [(m\pi a) \operatorname{cosech}^2(m\pi a) - (1-2\nu)(\coth(m\pi a) - 1)], \\
 L_3^1(y, z) &= \frac{\pi}{2} \sum_{m=1,2,\dots}^\infty \frac{\frac{2m\pi}{a^2}}{\sinh \frac{2m\pi}{a} + \frac{2m\pi}{a}} \frac{d}{dz} \left[ R\left(\frac{m\pi}{a}, z\right) \right] h_2\left(\frac{m\pi}{a}, y\right).
 \end{aligned}$$

$$L^2(y, z) = L_1^2(y, z) + L_2^2(y, z) - L_3^2(y, z), \quad (\text{C.5})$$

with

$$\begin{aligned}
 L_1^2(y, z) &= \frac{1-2\nu}{2} \left[ \int_0^\infty \exp(-s) \operatorname{cosech} s \sinh(sy) \cosh(sz) ds \right], \\
 L_2^2(y, z) &= \sum_{m=1,2,\dots}^\infty \sin(m\pi y) \cos(m\pi z) [(m\pi a) \operatorname{cosech}^2(m\pi a) - (1-2\nu)(\coth(m\pi a) - 1)], \\
 L_3^2(y, z) &= \sum_{m=1,2,\dots}^\infty \frac{\frac{2m\pi}{a^2}}{\sinh \frac{2m\pi}{a} + \frac{2m\pi}{a}} \frac{d}{dz} \left[ R\left(\frac{m\pi}{a}, z\right) \right] S\left(\frac{m\pi}{a}, y\right).
 \end{aligned}$$

$$H(c, z) = \left[ \frac{1-2\nu}{\pi} \int_c^1 \frac{y}{y^2 - z^2} dy - \int_c^1 L^2(y, z) dy \right] = H_1(c, z) - H_2(c, z), \quad (\text{C.6})$$

with

$$H_1(c, z) = \sum_{m=1,2,\dots}^{\infty} \frac{\cos(m\pi c) - \cos(m\pi)}{m\pi} \cos(m\pi z) [(m\pi a) \operatorname{cosech}^2(m\pi a) - (1 - 2\nu) \coth(m\pi a)],$$

$$H_2(c, z) = \sum_{m=1,2,\dots}^{\infty} \frac{\frac{2m\pi}{a^2}}{\sinh \frac{2m\pi}{a} + \frac{2m\pi}{a}} h_3\left(\frac{m\pi}{a}, c\right) \frac{d}{dz} \left[ R\left(\frac{m\pi}{a}, z\right) \right].$$

In all of the previous relations the following terms were used:

$$h_2(\lambda, t) = (\lambda \coth \lambda + 1 - 2\nu) I_0 - \lambda t I_1, \quad (C.7)$$

$$h_3(\lambda, t) = \frac{1}{\lambda^2} (\cosh \lambda - \cosh \lambda t) (\lambda \coth \lambda + (3 - 2\nu)) - \frac{1}{\lambda} (\sinh \lambda - t \sinh \lambda t), \quad (C.8)$$

$$S(\lambda, t) = R(\lambda, t) + 2(1 - \nu) \frac{\sinh(\lambda t)}{\lambda}, \quad (C.9)$$

$$R(\lambda, t) = \coth \lambda \sinh(\lambda t) - t \cosh(\lambda t). \quad (C.10)$$

## References

- 3M, 2015. Technical Guide. 3M<sup>TM</sup> VHB<sup>TM</sup> Structural Glazing Tape.
- Abramowitz, M., Stegun, I., 1964. Handbook of Mathematical Functions: With Formulas, Graphs, and Mathematical Tables. Applied Mathematics Series, Dover Publications.
- ASTM C1401-14, 2014. Standard Guide for Structural Sealant Glazing. ASTM International. West Conshohocken, PA.
- Barenblatt, G., 1962. The mathematical theory of equilibrium cracks in brittle fracture, Academic Press, New York, volume 7 of *Adv. Appl. Mech.*, pp. 55 – 129.
- Benveniste, Y., Miloh, T., 2001. Imperfect soft and stiff interfaces in two-dimensional elasticity. *Mech. Mat.* 33, 309–323.
- Buonsanti, M., Royer-Carfagni, G., 2003. From 3-d nonlinear elasticity theory to 1-d bars with nonconvex energy. *J. Elast.* 70, 87–100.
- Chatterjee, S.N., Prasad, S.N., 1973. On Papkovitch-Fadle solutions of crack problems relating to an elastic strip. *Int. J. Eng. Sci.* 11, 1079–1101.

- Chiu, P.K., Prasad, S.N., Dasgupta, S., 1976. Indentation of an elastic rectangle by a pair of rough punches with finite friction. *Int. J. Solids Struct.* 12, 619–634.
- Delincé, D., Sonck, D., Belis, J., Callewaert, D., Van Impe, R., 2008. Experimental investigation of the local bridging behaviour of the interlayer in broken laminated glass, in: *International Symposium on the Application of Architectural Glass ISAAG 2008 Conference Proceedings*, Munich, October 27-28, 2008, pp. 41–49.
- DowCorning®, 2015. DowCorning® Asia Construction Technical Manual. DowCorning.
- Dugdale, D., 1960. Yielding of steel sheets containing slits. *J. Mech. Phys. Solids* 8, 100 – 104.
- Ericksen, J., 1975. Equilibrium of bars. *J. Elast.* 5, 191–201.
- ETAG 002, 2012. Guideline For European Technical Approval For Structural Sealant Glazing Kits - Part 1: Supported and Unsupported Systems. European Organisation for Technical Approvals. november 1999 edition.
- Fadle, J., 1940. Die selbstspannungs-eigenwertfunktionen der quadratischen scheibe. *Arch. Appl. Mech.* 11, 125–149.
- Ferretti, D., Rossi, M., Royer-Carfagni, G., 2012. Through-cracked tensile delamination tests with photoelastic measurements, in: *Challenging Glass 3*, Bos, Freek; Louter, Christian; Nijse, Rob; Veer, Fred.
- Franco, A., Royer-Carfagni, G., 2014a. Cohesive debonding of a stiffener from an elastic substrate. *Comp. Struct.* 111, 401–414.
- Franco, A., Royer-Carfagni, G., 2014b. Effective bond length of FRP stiffeners. *Int. J. Non-Lin. Mech.* 60, 46–57.
- Hashin, Z., 2002. Thin interphase/imperfect interface in elasticity with application to coated fiber composites. *J. Mech. Phys. Solids* 50, 2509–2537.
- Hooper, C., 1964. Low-temperature elastic behavior of fourteen compounded elastomers. Technical Memorandum X-53137. Materials Division Propulsion And Vehicle Engineering Laboratory. NASA-George C. Marshall Space Flight Center, Huntsville, Alabama.

- Klarbring, A., 1991. Derivation of a model of adhesively bonded joints by the asymptotic expansion method. *Int. J. Eng. Sci.* 29, 493–512.
- Lebon, F., Rizzoni, R., 2011. Asymptotic behavior of a hard thin linear elastic interphase: An energy approach. *Int. J. Solids Struct.* 48, 441–449.
- Muralidhar, S., Jagota, A., Bennison, S., Saigal, S., 2000. Mechanical behaviour in tension of cracked glass bridged by an elastomeric ligament. *Acta Mater.* 48, 4577 – 4588.
- Needleman, A., 1987. Continuum model for void nucleation by inclusion debonding. *J. Appl. Mech.*, Transactions ASME 54, 525–531. Cited By 1139.
- Needleman, A., 1990. An analysis of tensile decohesion along an interface. *J. Mech. Phys. Solids* 38, 289 – 324.
- Needleman, A., 1992. Micromechanical modelling of interfacial decohesion. *Ultramicroscopy* 40, 203 – 214.
- Papkovich, P., 1940. On one form of solution of the plane problem of the theory of elasticity for a rectangular strip, in: *Dokl. Akad. Nauk SSSR*, pp. 335–339. In Russian.
- Prasad, S., Dasgupta, S., 1975. Effect of sliding friction on contact stresses in a rectangle compressed by rigid planes. *J. Appl. Mech.* 42, 656–662.
- Prasad, S.N., Chatterjee, S.N., 1973. Some mixed boundary value problems of elasticity in a rectangular domain. *Int. J. Solids Struct.* 9, 1193–1210.
- Raous, M., 2011. Interface models coupling adhesion and friction. *CR Mécanique* 339, 491 – 501. Surface mechanics : facts and numerical models.
- Sneddon, I.N., 1966. Mixed boundary value problems in potential theory. North-Holland.
- Tvergaard, V., Hutchinson, J.W., 1993. The influence of plasticity on mixed mode interface toughness. *J. Mech. Phys. Solids* 41, 1119 – 1135.
- Tvergaard, V., Hutchinson, J.W., 1994. Toughness of an interface along a thin ductile layer joining elastic solids. *Philos. Mag. A* 70, 641–656.



Ward, I., Sweeney, J., 2005. An Introduction to the Mechanical Properties of Solid Polymers. Wiley.

Xu, X.P., Needleman, A., 1994. Numerical simulations of fast crack growth in brittle solids. J. Mech. Phys. Solids 42, 1397 – 1434.

ACCEPTED MANUSCRIPT